Molecular Structural Analysis of Hydrated Ethylene Glycol Accounting for the Antifreeze Effect by Using Infrared Attenuated Total Reflection Spectroscopy

Takafumi Shimoaka[a] and Takeshi Hasegawa[a†]

a. Laboratory of Solution and Interface Chemistry, Division of Environmental Chemistry, Institute for Chemical Research, Kyoto University, Gokasho, Uji, Kyoto 611-0011, Japan.

[†]Corresponding author: E-mail: htakeshi@scl.kyoto-u.ac.jp FAX: +81 774 38 3074

Graphical abstracts (5 cm x 13 cm)

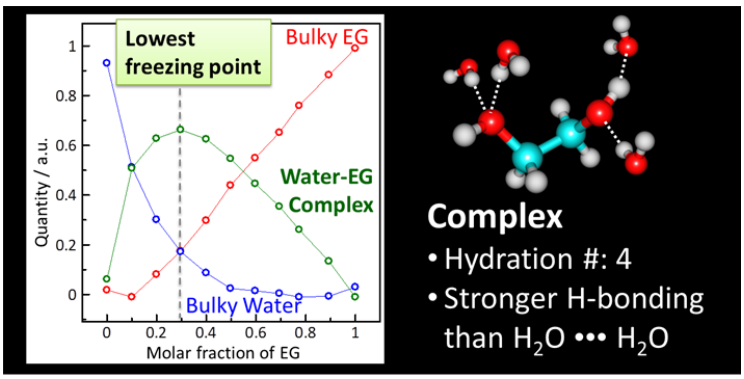

Abstract:

To reveal the antifreeze protection mechanism of an aqueous solution of ethylene glycol (EG) at a molecular level, concentration-dependent infrared spectra are analyzed with an aid of chemometrics. The principal component analysis (PCA) of the spectra reveals that the spectral variation is explained by the quantity changes not only of 'bulky water' and the 'bulky EG,' but also of a 'water/EG complex.' After a spectral decomposition using the alternative least squares (ALS) analysis, the spectrum of the complex reveals that the EG molecule keeps the gauche conformation, and the terminal hydroxyl groups are hydrogen bonded by water molecules, which is a key to understand the antifreeze effect. In addition, the complex is found to comprises an EG molecule with four water molecules. Since the quantity of the complex attains the maximum at an EG concentration of 60 wt%, at which the freezing point becomes lowest, the complex is concluded to be a key hydrated species for the antifreeze effect. The generation process of the water/EG complex is also studied by using the time-resolved IR spectroscopy, which consistently confirms the spectral discussion made above.

Keywords: Infrared Spectroscopy, Chemometrics, Ethylene Glycol (EG), Antifreeze Effect, Water/EG Complex

1. Introduction

An aqueous solution of ethylene glycol (EG) is used as an antifreeze solution for various purposes represented by the heat carrier medium in the radiator of a car engine, since the mixed solution shows an extremely lower freezing point (< -50 °C) than those of pure water and pure EG, which are frozen at 0 °C and -12.6 °C, respectively, at an ambient pressure. The antifreeze effect has been known to exhibit the best performance at an EG molar fraction (x_{EG}) of 0.29 (≈ 60 wt%) exhibiting the lowest freezing point[1,2]. Although the phase diagram of EG-water is typical for a binary solution, 'double eutectic points' are found at x_{EG} = 0.29 and 0.55, which indicates a formation of a 'hydrated species' in the concentration range between the two eutectic points. Since the concentration exhibiting the lowest freezing point appears in the concentration range, the hydrated species has a relation to the antifreeze effect. The molecular picture accounting for the effect and the molecular structure of the species in the mixture has, however, never been revealed thus far.

To reveal the chemical mechanism of the antifreeze effect, thermodynamic properties as a function of the concentration have extensively been investigated [3-8]. In particular, excess molar enthalpy (ΔH^E) and entropy (ΔS^E) at an ambient pressure are discussed in detail, since these parameters with the concentration have a similar trend to that of the freezing point, which has the minimum value at the x_{EG} of 0.29. For example, ΔH^E is always exothermic ($\Delta H^E < 0$) in the full concentration range having the minimum value at $x_{EG} \approx 0.3$ [3,4]. This indicates that the solution releases heat energy during the mixing process, which suggests that an energetically stable hydrated species consisted of the water and

EG molecules are generated in the mixed solution especially at the concentration. On the other hand, the excess molar entropy, ΔS^{E} , which is estimated by the subtraction between the excess free energy, ΔG^{E}, and ΔH^{E} [5], is also negative in the concentration range, implying an incomplete mixing at a molecular level [9,10]. Of interest is that ΔS^{E} also shows minimum at $x_{EG} \approx 0.3$. Therefore, pure water and EG should not be mixed homogeneously, but instead another metastable hydrated species should be generated. The volume scale of the homogeneous region of molecular order, however, cannot be discussed only by the thermodynamic measurements unfortunately.

To connect the thermodynamic properties with a molecular image, spectroscopic studies have already been reported. For example, nuclear magnetic resonance (NMR) was employed to determine the rotational correlation time of water molecules in the solution in a low concentration range of EG (0~7 wt%), and unusually motion-restricted water molecules were found [11]. Judging from the correlation time, the number of hydration water molecules about an EG molecule was also estimated to be 5.7. Since the number of hydration water molecules is revealed only in a low concentration range up to 7 wt% ($x_{EG} < 0.021$), however, the results cannot explain the antifreeze effect unfortunately.

The conformation of the EG molecule in an aqueous solution was also investigated by using NMR [11,12], vibrational spectroscopy [13] and large-angle X-ray scattering (LAXS) [14]. They reached a common conclusion that the most of EG molecules takes the gauche conformation, in which the dihedral angle of O-C-C-O is close to ±60°. In addition, Pachler and co-workers investigated the conformational population of EG molecules using NMR, and revealed that 88% of the EG molecules

take the gauche conformation in an aqueous solution of EG at a molar fraction of x_{EG} = 0.1 [12]. They also discussed pure EG, and revealed that 86% of the EG molecules take the gauche conformation even though they are hydrogen bonded with each other like water. These results indicate that the conformation of an EG molecule is impervious to the dissolution in water. In this way, the molecular conformation of EG involved in water is well known. No correlation, however, between the molecular conformation and the thermodynamic properties associated with the antifreeze effect is available yet.

With the LAXS data [14], the number of hydrogen bonds per molecule were readily evaluated via the radial distribution functions. The number *linearly* changes from ca. 3.5 (pure water) to ca. 2.0 (pure EG) with the concentration. Therefore, due to the LAXS analysis, the water and EG molecules seems to be mixed homogeneously. However, the homogeneous mixing cannot explain the thermodynamic properties exhibiting a minimum as mentioned above. In this way, the mechanism of the antifreeze effect is still an unresolved matter, although the many molecular pictures are proposed. This may be because NMR and LAXS measurements provide the averaged information of the molecules in the solution. If the antifreeze effect is caused by a small amount of a metastable hydrated species, which induces the exothermic mixing, information of the minor species in a measured data should be hidden in the averaged information. Therefore, it is necessary to decompose the mixed information into that of each species involved in the solution.

In the present study, aqueous solutions of EG with various concentrations are studied by infrared attenuated total reflection (IR ATR) spectroscopy. A chemometric analysis of the spectra reveals that

the solution involves “three” distinguishable species. In fact, the spectra are readily decomposed into three spectra: a newly found spectrum of a chemical complex of water and EG as well as the pure water and EG spectra. The amount of the chemical complex exhibits the maximum at the EG concentration of 60 wt%, which straightforwardly implies that the complex is the key to account for the antifreeze effect. As a result, the ‘EG molecule in the complex’ is found to be H-bonded by about four water molecules, although the ‘pure EG’ molecules are imperfectly H-bonded. In addition, rapid scanning Fourier transform (FT) IR spectrometry is employed to pursue a mixing process of EG and water, and the mixing process with time toward an equilibrium state is also investigated.

2. Experimental

2.1. Chemicals

Pure EG was purchased from Wako chemicals (Osaka, Japan), and it was used without further purification. Pure water was obtained by a Millipore (Molsheim, France) Elix UV-3 pure-water generator and a Yamato (Tokyo, Japan) Autopure WT100U water purifier being compatible with Milli-Q. The water exhibited an electric resistivity of > 18.2 MΩ cm, and the surface tension was 72.5 mN m^{-1} at 25 °C, which was measured by using a Kyowa Interface Science Co., Ltd. (Saitama, Japan) DropMaster, DM-501Hy, contact-angle meter.

2.2. IR Measurements

All the infrared spectra were measured by a Thermo-Fisher Scientific (Madison, WI, USA) Nicolet 6700 Fourier transform infrared (FT-IR) spectrometer using a Spectra-Tech (Oak Ridge, TN,

USA) Foundation Performer single-reflection ATR accessory having a hemisphere-shaped germanium prism. The inside of the spectrometer was air purged by flowing a dry air generated by an Air-Tech (Yokohama, Japan) AT-35H dried-air generator, after passing through a molecular sieve tower after the generator. A liquid-nitrogen cooled Hg-Cd-Te (MCT) detector was used. Concentration dependent IR spectra were recorded by coaddition of 1000 interferograms at a wavenumber resolution of 4 cm^{-1} with a modulation frequency of 60 kHz. Time-resolved spectra without an accumulation were recorded by the rapid-scanning mode with a wavenumber resolution of 4 cm^{-1} with a modulation frequency of 200 kHz. The time interval of the successive IR measurements was 0.18 sec.

2.3. Chemometrics

To obtain chemically independent spectra from the concentration dependent IR spectra, alternative least-squares (ALS) regression were performed after principal component analysis (PCA) [15,16], which can estimate the number of constituents. In the analysis of time-resolved spectra without an accumulation, the spectral noise was significantly reduced by the use of PCA, which were used for the classical least square (CLS) regression analysis. The chemometrics calculations of PCA, CLS and ALS regression were performed on Mathworks (Natick, MA) MATLAB ver. R2014b by using homemade programs.

3. Results and Discussion:

3.1. Molecular Mechanism of the Antifreeze Effect of an Aqueous Solution of EG

3.1.1. Concentration Dependent IR Spectra of an Aqueous Solution of EG. Fig. 1 presents the concentration dependent IR spectra of an aqueous solution of EG at ambient temperature. The similar spectral variation is obtained in a past research [17]. The spectra presented by the blue and red curves correspond to pure water (x_{EG} = 0.0) and EG (x_{EG} = 1.0), respectively. With increasing the concentration of EG, the OH_2 bending vibration ($\delta(OH_2)$) band of water at ca. 1640 cm^{-1} decreases and disappears; whereas the CH_2 stretching vibration ($\nu(CH_2)$) band and the CO stretching vibration (ν(CO)) band develop. The OH stretching vibration (ν(OH)) bands of both water and EG have a broad shape, and the band shape gradually changes from that of pure water to EG, which seems that the hydrogen(H)-bonding state in the solution changes in a continuous manner. It is worth noting that several isosbestic points apparently appear in the spectra, which are marked by yellow circles in Fig. 1. This suggests that the spectral variation may be explained by the quantity changes of two chemical constituents; water and EG. The $\nu(CH_2)$ and $\delta(OH_2)$ bands show a peak shift, however, which indicates that the H-bonding state in the mixed solution is different from those of pure water and EG. This suggests that an additional minor constituent should be considered to fully explain the spectral variation.

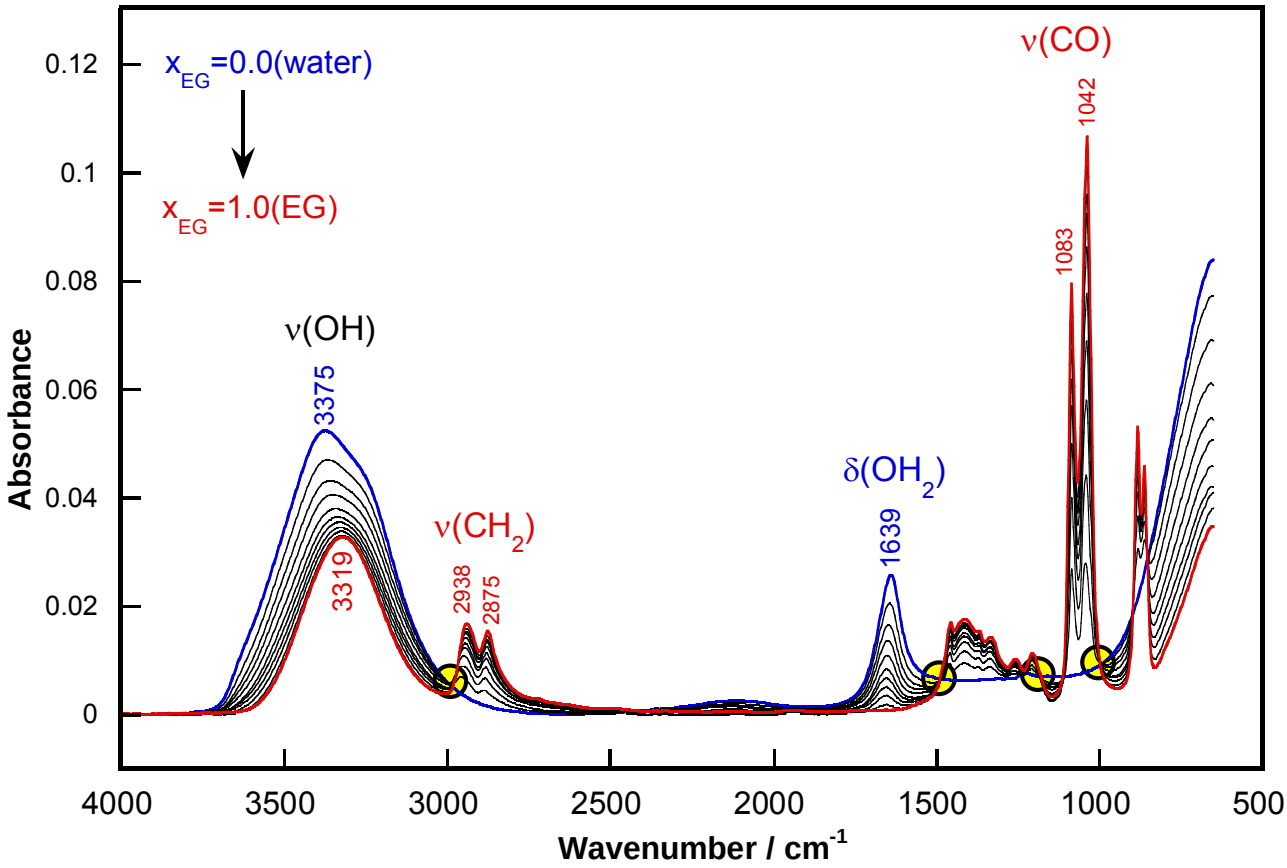

Fig. 1 Concentration dependent IR ATR spectra of the EG aqueous solution from x_{EG}=0.0 (pure water) to 1.0 (pure EG). The yellow circles exhibit the isosbestic-like cross points.

3.1.2 Chemometric Analysis of the IR Spectra. To estimate the appropriate number of chemical constituents for fully explaining the spectral change, the principal component analysis (PCA) is employed, which is expressed by Eq(1).

$$\mathbf{A} = \begin{bmatrix} \mathbf{a}_1 \\ \mathbf{a}_2 \\ \vdots \\ \mathbf{a}_{11} \end{bmatrix} = \mathbf{t}_1\mathbf{p}_1 + \mathbf{t}_2\mathbf{p}_2 + \cdots + \mathbf{t}_{11}\mathbf{p}_{11} \qquad (1)$$

The matrix, **A**, in Eq(1) consists of all the spectral data in Fig. 1. For example, the absorbance spectrum of pure water is stored as a row-wise vector, $\mathbf{a}_1$. PCA expands the matrix, **A**, using mutually orthogonal loading vectors, $\mathbf{p}_i$. The number of the expanded terms is equal to the number of rows in **A** (i = 1~11). Each loading vector, $\mathbf{p}_i$, has the corresponding eigenvalue, λ_i, which satisfies Eq(2).

$$\mathbf{A}^{\mathrm{T}}\mathbf{A}\mathbf{p}_i = \lambda_i \mathbf{p}_i \qquad (2)$$

Here, $\mathbf{A}^{\mathrm{T}}$ is the transpose matrix of **A**. The eigenvalue, λ_i, is useful to estimate the number of constituents, since the eigenvalue is the variation of the spectral points spread in multi-dimensional space along the loading vector, which is also the degree of contribution of $\mathbf{p}_i$ to the matrix **A**. In the present analysis, the wavenumber region of 4000–1150 cm^{-1} after an appropriate baseline correction is used, which involves the key bands exhibiting a significant shift [17]. In Fig. 2a, the eigenvalues are plotted as a function of the factor rank, i. The first three loading vectors ($\mathbf{p}_i$: i = 1~3) are presented as spectra in Fig. 2b. Although the spectra are not chemically meaningful in principle, they are all noise free, and the corresponding eigenvalues apparently indicate that "three" factors are necessary for the PCA modeling, which agrees with the conclusion of the previous section. The contribution ratios of the first three principal components, r_n, calculated with the equation of $r_n = \lambda_n / \sum_{i=1}^{11} \lambda_i \times 100$, are 82.1 % ($n$=1), 15.3 % ($n$=2) and 1.8 % ($n$=3). In this manner, the matrix, **A**, is mostly modeled by only the 1st and 2nd principal components (97.3 %), this is why the isosbestic point-like cross points appear in Fig. 1. The newly found 3rd component is, however, necessary to explain the peak shift in the $\nu(CH_2)$ and $\delta(OH_2)$ region, which may be related to an additional constituent generated in the mixed solution.

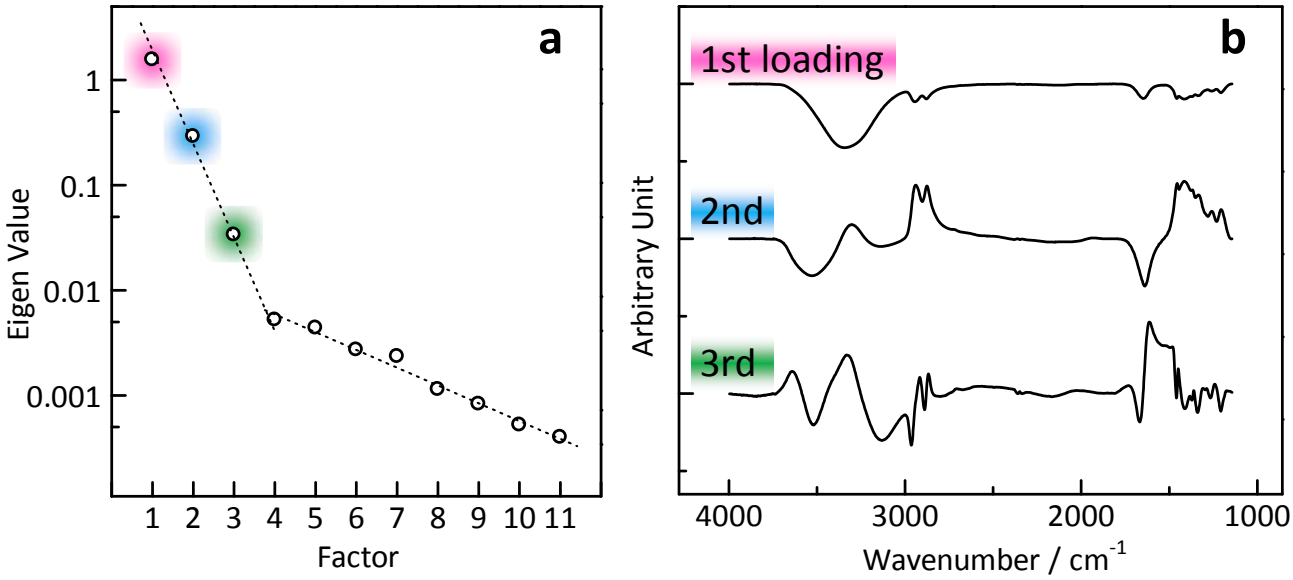

Fig. 2 Calculated results of the PCA analysis: (a) Eigenvalues, λ, plotted against the factor rank, i in a semi-log graph. (b) First three loading vectors ($\mathbf{p}_i$: i = 1~3).

To reveal the spectra of the three constituents, the ALS technique was employed. ALS is the one of the multivariate curve resolution (MCR) techniques based on the CLS regression [19-21]. The matrix, **A**, are modeled by a linear combination of spectroscopically independent three spectra ($\mathbf{k}_1$, $\mathbf{k}_2$, $\mathbf{k}_3$) and the concentration matrix, **C** (Eq. (3)).

$$\mathbf{A} = \begin{bmatrix} \mathbf{a}_1 \\ \mathbf{a}_2 \\ \vdots \\ \mathbf{a}_{11} \end{bmatrix} = \begin{bmatrix} c_{1,1} & c_{1,2} & c_{1,3} \\ c_{2,1} & c_{2,2} & c_{2,3} \\ \vdots & \vdots & \vdots \\ c_{11,1} & c_{11,2} & c_{11,3} \end{bmatrix} \begin{bmatrix} \mathbf{k}_1 \\ \mathbf{k}_2 \\ \mathbf{k}_3 \end{bmatrix} + \mathbf{R} \qquad (3)$$

Since the total concentration is normalized to be unity ($c_{i,1} + c_{i,2} + c_{i,3} \approx 1$) in the algorithm for a fast convergence, the each concentration, $c_{i,j}$, indicates a contribution of the corresponding spectrum, $\mathbf{k}_j$,

to the spectrum, $\mathbf{a}_i$. In other words, a quantitative change of each pure-constituent as a function of x_{EG} is recorded column-wisely in the matrix, **C**. Here, **R** is a matrix that receives nonlinear residuals. In the case of CLS, two of the three matrices (**A**, **C**, **K**) must be known in advance to solve the rest unknown matrix. In our case, however, both **K** and **C** are unknown, and only the spectra matrix, **A**, is available, for which ALS works powerful. ALS yields the converged solution for both matrices, **C** and **K**, under the non-negative constraint [19-22]. As a result, ALS yields relative values, and the variation shapes are accurately generated, i.e., the concentration profile and the spectral shapes are readily obtained as presented in Fig. 3.

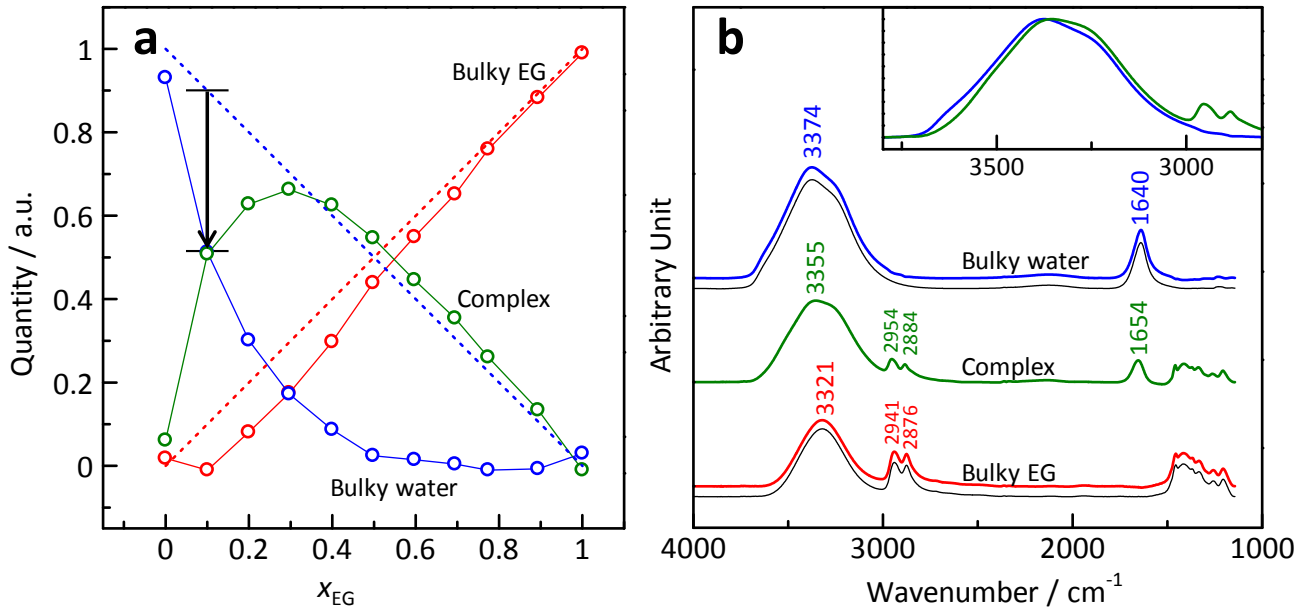

Fig. 3 (a) The quantity variations of the three constituents yielded by the ALS calculation: bulky water (blue), bulky EG (red), and the complex (green), as a function of x_{EG}. Theoretical quantities of water and EG in an ideal mixing are presented by the blue and red dotted lines, respectively. (b) The corresponding spectra of the three constituents are presented with the same color as used in (a). Spectra presented by black line beneath the blue and red ones are the spectra of pure water and EG, respectively. The ν(OH) bands of bulky water and the complex are overlaid in the inset.

In Fig. 3a, the obtained matrix, **C**, is presented as a function of x_{EG}. In a similar manner, the corresponding spectra are presented in Fig. 3b. The blue spectrum decomposed by ALS agrees with the pure-water spectrum (black spectrum beneath the blue one) in Fig. 3b. The corresponding quantity shown by the blue line in Fig. 3a decreases monotonously with an increase of x_{EG}. These results indicate that the solution involves 'bulky water' up to the concentration of ca. $x_{EG} = 0.5$, in which the H-bonding state is similar to that of pure water. Another constituent presented by the red line increases monotonously in Fig. 3a, and the corresponding spectrum is almost identical to that of pure EG as presented in Fig. 3b. The 'bulky EG' is thus found to appear when the concentration of x_{EG} is 0.2 or higher. The rest third constituent (green line) shows the maximum at x_{EG} of 0.3. Since the green curve is nearly zero at $x_{EG} = 0$ (pure water) and $x_{EG} = 1$ (pure EG), the third constituent is assigned to a product that is newly generated from water and EG. The corresponding green spectrum in Fig. 3b has, in fact, the key bands of both water ($\delta(OH_2)$) and EG ($\nu(CH_2)$). The third constituent is thus concluded to be a 'complex' of water and EG molecules. Note that $x_{EG} = 0.3$ corresponds to the concentration exhibiting the lowest freezing point, at which the excess molar enthalpy exhibits the minimum value (see Introduction). This implies that the complex exhibiting the green spectrum is thermodynamically stable.

The decomposed spectra by ALS are known to be not suitable for further quantitative discussion in principle [15]. Since the spectra of bulky water and EG shown in Fig. 3b agree with those of pure water and EG not only for the shape, but for 'intensity,' the quantity of only bulky water and EG shown

in Fig. 3a can limitedly be converted to the number of molecules fortunately. In particular, the spectrum of pure water (x_{EG} = 0.0) can be explained by only the spectrum of bulky water ($\mathbf{A}_{0.0} \approx 1.0\mathbf{k}_{water}$).This indicates that the relative number of water molecules in the mixed solution can be estimated by using the blue curve in Fig. 3a. In a similar manner, the average molar ratio of the complex can be estimated by considering that the bulky EG is completely lost in the range of x_{EG} = 0.0 ~ 0.1 as shown by the red curve. As a result, the quantities of the bulky water and EG are both found to have 0.5 (Fig. 3a) at x_{EG} = 0.1 (i.e., x_{water} = 0.9).

Therefore, the spectrum at x_{EG} = 0.1 in Fig. 1 can be modeled by summation of the spectra of the bulky water and the complex with a common intensity of 0.5 ($\mathbf{A}_{0.1} \approx 0.5\mathbf{k}_{water} + 0.5\mathbf{k}_{complex}$). On the blue theoretical dotted line at x_{EG} = 0.1, the quantity of water molecules is read to be 0.9. Since some of the water is exhausted to generate the complex exhibiting 0.5, the quantity of the used water is 0.4 as indicated by the arrow in Fig. 3a. Considering x_{EG} = 0.1, the molar ratio of EG to water in the complex is thus revealed to be ca. 1:4, which can roughly be used as an index of the hydration of molecules in motion.

In this manner, the ALS analysis reveals that (1) an EG molecule in the complex is hydrated by about four water molecules, and (2) the complex should be a key species to induce the antifreeze effect. The thermodynamic relationship between the complex and the antifreeze effect will be discussed next.

3.1.3 Molecular Structure and Hydrogen-Bonding State of the Complex. To reveal the relationship between the complex and the antifreeze effect, the spectrum shown in Fig. 3b is discussed in detail. First, the $\delta(OH_2)$ band is located at 1654 cm^{-1}, which is 14 cm^{-1} higher than that of pure water. Since the $\delta(OH_2)$ band is known to appear at a higher position when the H-bonding becomes stronger, the H-bonding in the complex should be stronger than that in pure water. Since an EG molecule in the complex is hydrated by about four water molecules, the strong H-bond is assigned to the intermolecular interaction between the EG and water molecules.

The $\nu(OH)$ band of the complex having a similar shape to that of bulky water is too broad to make a fine discussion using the peak position. In the inset of Fig. 3b, the two bands of bulky water and the complex are overlaid on each other, which implies that the complex band is entirely shifted to a lower wavenumber. Since the $\nu(OH)$ band is known to shift to a lower wavenumber when the H-bonding becomes stronger, the H-bonding in the complex is stronger than that in bulky water, which is the same trend as that of the $\delta(OH_2)$ region. In this manner, the EG/water complex has spectroscopically proved to be stabilized by the H-bonding.

Another notable point is found in the $\nu(CH)$ band region, in which the symmetric and antisymmetric CH_2 stretching vibration ($\nu_s(CH_2)$ and $\nu_a(CH_2)$) bands of the complex appear at a higher wavenumber (2884 and 2954 cm^{-1}) than those of bulky EG (2876 and 2941 cm^{-1}). Two possible reasons for the shift are: a conformational change of the EG molecule and a change of the H-bonding state about the EG molecule.

As mentioned in Introduction, the conformation of the EG molecule in an aqueous solution has already been discussed by many researchers, and the dominant conformation is 'gauche' *irrespective of the EG concentration*. It is especially important that an EG molecule is easily accommodated in the H-bonding network of water, since the distance between two oxygen atoms ($r_{O\cdots O}$) in the gauche EG molecule, 2.9 Å, is similar to the nearest neighboring $r_{O\cdots O}$ of water (2.85 Å), which results in favorable enthalpic interactions between the ether oxygen and water without disturbing the H-bonding network of water [22]. Therefore, the higher wavenumber shift *cannot* be attributed to the conformational change of the EG molecules.

In a former study, we investigated the influence of the H-bonding about the OH group of methanol using the ν(CH) band position of the methyl group [24][24]. The OH group has two proton accepter sites on the oxygen atom and one proton donor site. The quantum chemical calculation of a variety of methanol clusters revealed a correlation tendency of the ν(CH) wavenumber with the hydration numbers at both H-bonding sites. As a result, only the methanol having H-bonding-free lone pairs on oxygen exhibits an extremely lower band position than a H-bonded methanol by 30 cm^{-1}. Since the electronic state of the methylene group of EG should be similar to that of methanol, the same rule can be applied to the discussion of the ν(CH) band of EG in Fig. 3b.

The $\nu_s(CH_2)$ and $\nu_a(CH_2)$ bands of the EG/water complex appear at a higher wavenumber position by 8 and 13 cm^{-1} than those of bulky EG respectively. This indicates that the EG molecule in the complex is more H-bonded than that in bulky EG, but the both shifts are apparently smaller than 30 cm^{-1}, which

suggests that no EG molecules should have H-bond-free lone pairs on oxygen in bulky EG. According to LAXS measurements of pure EG, in fact, the number of H-bonds per molecule is ca. 2.0 [14], which indicates that two of the six H-bonding sites of an EG molecule are already occupied by neighboring EG molecules.

3.1.4 Understanding of the Antifreeze Effect in the Phase Diagram. The mechanism of the antifreeze effect is discussed by taking the EG/water complex into consideration. In Fig. 4b, the phase diagram (x_{EG}-Temperature) of the EG aqueous solution reported by Bevan Ott et al. is presented [2]. The line along the circle (○) indicates the freezing curve, and the region above the freezing curve corresponds to the liquid phase, *L* comprised of water and EG. The phase diagram indicates that the solidification process depends on the three distinct x_{EG} ranges, (1) from 0 to 0.29 (2) from 0.29 to 0.54 (3) from 0.54 to 1.

In Fig. 4a, the quantities of the three constituents revealed in the present study are re-presented. The quantity of the complex shows the maximum at x_{EG} = 0.29, which is in the concentration range of (2). According to the phase diagram, the solution in this range becomes solidified in one step without squeezing out pure water and EG, which corresponds to the solid solution, *S*. In this concentration range at an ambient temperature, the bulky constituents of both water and EG are minor (see Fig. 4a). Since the complex is energetically stable, it is not dissociated to be back to pure water, which preserves the

low freezing point. This is consistent with a fact that the H-bonding network like ice I_h does not develop in a solution of the complex.

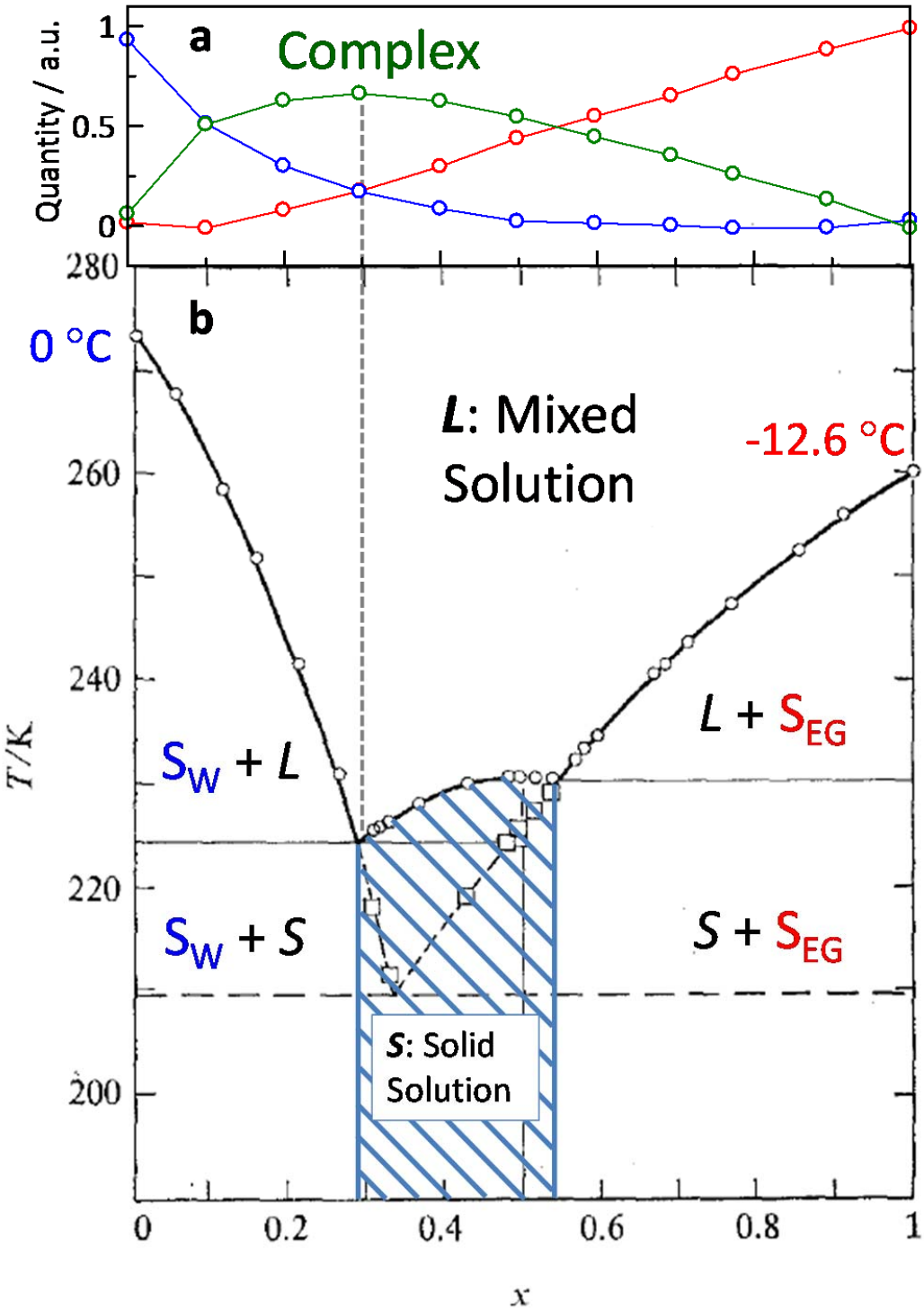

Fig. 4 (a) The quantity variations of the three constituents against x_{EG}. (b) The phase diagram of an EG aqueous solution reported by Bevan Ott et al. [Reprinted with permission from J. Bevan Ott et al. *The Journal of Chemical Thermodynamics*, **4**, 123-126, Figure 1, Copyright © 1972 Published by Elsevier]

3.2. Mixing Process of EG and Water toward Equilibrium

In the previous sections, mixed solutions of the three constituents after reaching equilibrium are discussed. Since the complex is generated as a result of mixing water and EG, the generation process is of another interest. In this section, the mixing process is studied by using time-resolved IR spectroscopy.

Time-resolved IR ATR spectra of the mixing process were measured by using the rapid-scan mode of FT-IR every 0.18 sec. At the time of 10 sec after starting the IR measurements of pure EG, water was added to the sample, and the mixing process was pursued for 50 sec at the concentration of $x_{EG} = 0.2$ (EG: 564 μL and water: 436 μL). The total number of the collected spectra is 360, and several selected spectra are presented in Fig. 5a. The first spectrum at 10.115 sec is almost identical to that of pure EG in Fig. 1 (x_{EG}=1.0), and no influence of water is found at this moment. Later, the key bands of EG (e.g., $\nu_s(CH_2)$ and $\nu_a(CH_2)$) decrease and the $\delta(OH_2)$ band of water appears, and the spectra at 30.035 sec or later are almost identical to the spectrum in the equilibrium state at x_{EG}=0.2 in Fig. 1. The absorbance of the $\delta(OH_2)$ band of water at 1648 cm^{-1} is plotted against time in Fig. 5b. The absorbance stays at nil until ca. 14 sec, and it rapidly increases until ca. 20 sec, after which the solution seems to reach the equilibrium. No more detail, however, can be discussed on these figures, since much noise is involved.

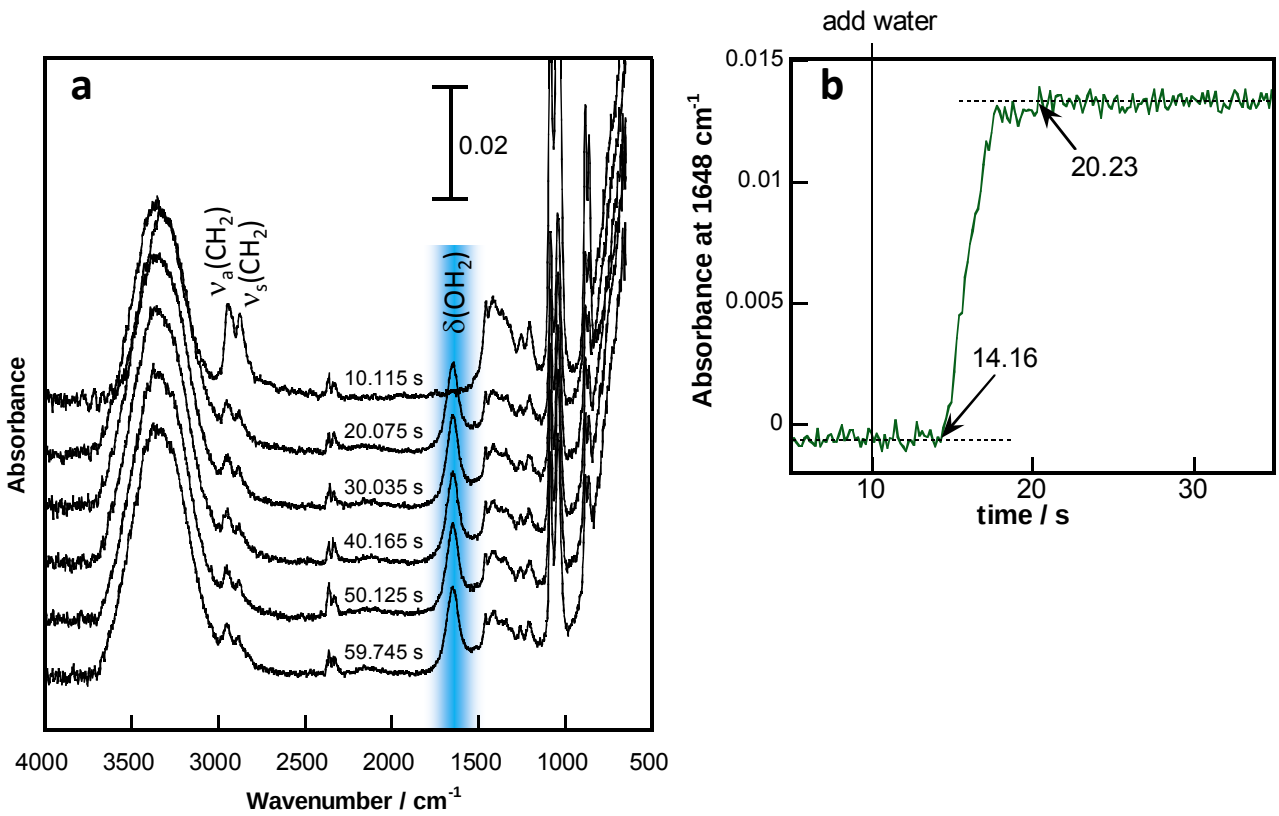

Fig. 5 (a) Selected time-resolved IR ATR spectra from 10.115 to 59.745 sec. (b) The time-dependent absorbance at the $\delta(OH_2)$ band of water at 1648 cm^{-1}.

To remove noise from the collection of many spectra, PCA was employed. The 360 time-resolved spectra are stored in the matrix, $\mathbf{A}_t$, and the matrix is expanded by the mutually orthogonal loading vectors $\mathbf{p}_i$ (Eq (1)).

The first 40 eigenvalues are presented in Fig. 6a. The loading spectra by PCA (data not shown) indicated that the first eight vectors (p_i: i = 1~8) involved a chemically meaningful signal correlated with the vibration bands of water and/or EG; whereas the rest loading vectors (p_i: i > 8) are only of noise. Therefore, the first eight factors are recognized as the 'basis factors'; whereas the rest factors are

‘noise factors.’ The noise-reduced new matrix, $\mathbf{A}_{rec}$, is reconstructed by using the basis factors only. Fig. 6b presents the noise-reduced spectra. Since the noise on the spectra is readily reduced apparently, the spectra are ready for further spectral analysis. Judging from the eigenvalues in Fig. 6a, three constituents are significant, which agrees with the results of the equilibrium study. The constituents should thus be assigned to the bulky water, bulky EG and the water/EG complex. If the assignments are true, a CLS analysis (Eq. (4)) would work well using the **K** matrix consisted of the three spectra shown in Fig. 3b.

$$\mathbf{A}_{rec} = \mathbf{CK} + \mathbf{R} \qquad (4)$$

CLS has a great benefit that the variation of each constituent is quantitatively appeared in **C**, if the number of constituents and the assignments are both true. The unknown matrix, **C,** is obtained as the least-squares solution by using Eq. (5),

$$\mathbf{C} = \mathbf{A}_{rec}\mathbf{K}^{T}(\mathbf{KK}^{T})^{-1} \qquad (5)$$

and the results are presented in Fig. 7 with time. CLS has an important characteristic that the analytical results would be severely degraded, if a wrong number of constituents are used for the calculation. As a matter of fact, the calculated results in Fig. 7 are quite reasonable, and the quantity change of the bulky water (blue curve) agrees well with the curve in Fig. 5b. In this manner, the mixing of water and EG is thus concluded to generate a three-constituent system. The reasonable curves paradoxically confirm that the pure constituent spectra in Fig. 3b are also correct.

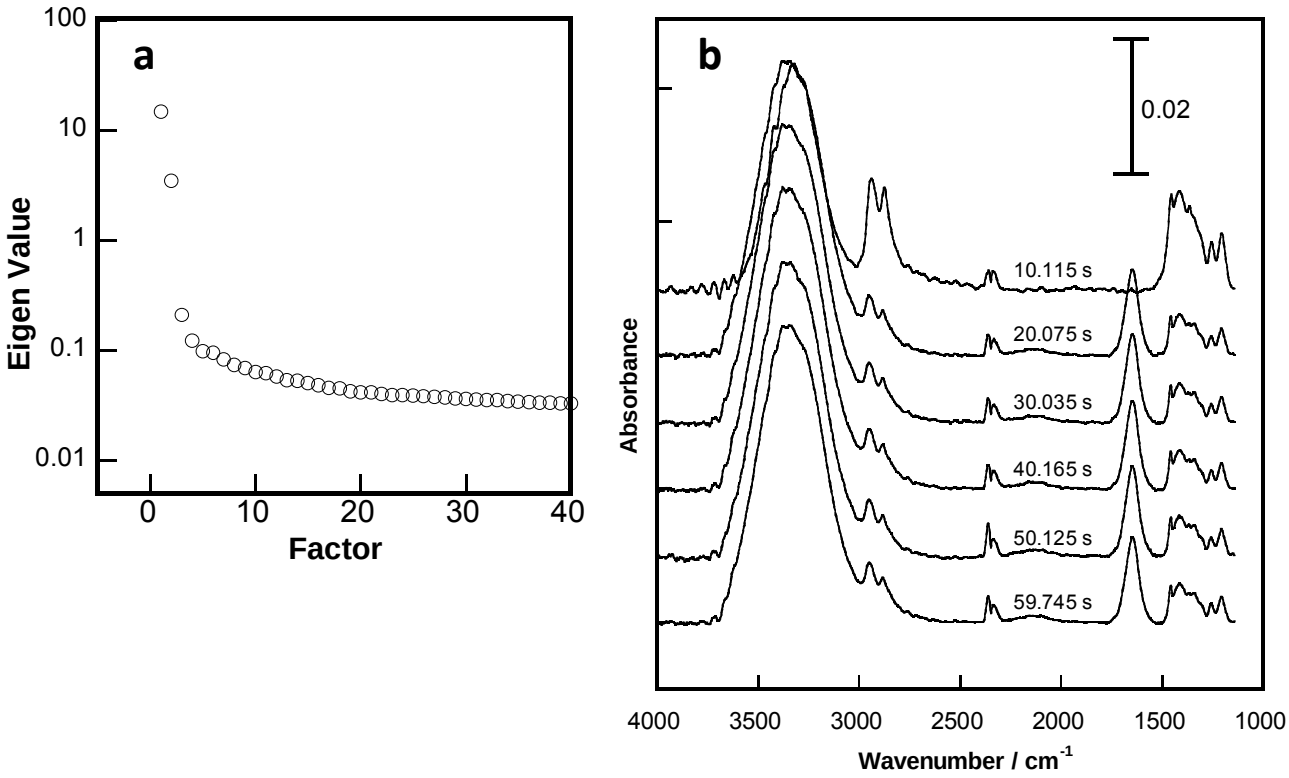

Fig. 6 Calculated results of the PCA analysis of the time-resolved spectra: (a) Eigenvalues, λ, plotted against the factor rank, i, in a semi-logarithmic manner (i = 1~40). (b) The noise-reduced spectra regenerated by using the first eight basis factors ($\mathbf{p}_i$: i = 1~8).

The results in Fig. 7 show that the bulky EG is largely lost, and the added water is also largely used to generate the complex as the dominant species after reaching the equilibrium at x_{EG} = 0.2, which reproduces the result in Fig. 3a.

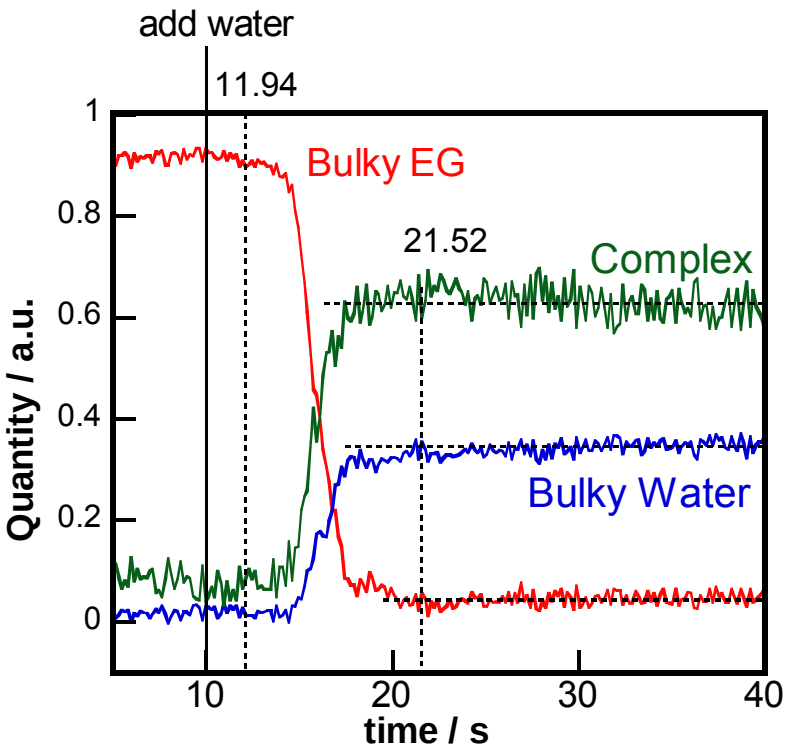

Fig. 7 The time-dependent quantities of the three constituents calculated by the CLS regression.

4. Conclusion

Concentration-dependent IR spectra of an aqueous solution of EG were analyzed with an aid of chemometrics to study the antifreeze protection mechanism of at a molecular level. PCA analysis of the spectra indicates that 'three' constituents are necessary for modeling the spectral variation. The ALS analysis considering three constituents was successfully performed, and the result indicated that an EG aqueous solution involves a 'complex' of the water and EG molecules as well as 'bulky water' and 'bulky EG,' in which each H-bonding state is similar to that of pure water and EG. Since the quantity of

the complex shows the maximum at the EG molar fraction of 0.3, at which the freezing point reaches the minimum, the complex is concluded to be the key hydrated species for understanding the antifreeze effect. After considering the former studies on quantum chemical calculation in a similar system, the 'complex' has been revealed that: (1) EG molecule in the complex is hydrated by about four water molecules, although the OH group forms imperfect H-bonding even in pure EG and (2) H-bonding in the complex is stronger than that in pure water. The generation process of the water/EG complex during the mixing of water and EG was also studied by using the time-resolved IR spectroscopy. The spectra in the mixing process are readily explained by using the decomposed three spectra in the equilibrium study above on a CLS regression analysis, which confirms that the results obtained by ALS are consistently reasonable. In this manner, the generation of the water/EG complex is concluded to be a key species to account for the antifreeze effect.

Acknowledgment: This work was financially supported by Grant-in-Aid for Scientific Research (B) [No. 23350031] from Japan Society for the Promotion of Science, and Priority Areas [No. 23106710) from the Ministry of Education, Science, Sports, Culture, and Technology, Japan.

References and Notes

[1] D. R. Cordray, L. R. Kaplan, P. M. Woyciesjes and T. F. Kozak, *Fluid Phase Equilibria*, 1996, **117**, 146-152.

[2] J. Bevan Ott, J. Rex Goates and John D. Lamb, *J. Chem. Thermodynamics*, 1972, **4**, 123-126.

[3] J.-Y. Huot, E. Battistel, R. Lumry, G. Villeneuve, J.-F. Lavallee, A. Anusiem and C. A Jolicoeur, *Journal of Solution Chemistry*, 1988, **17(7)**, 601-636.

[4] Y. Matsumoto, H. Touhara, K. Nakanishi and N. Watanabe, *J. Chem. Thermodynamics*, 1977, **9**, 801-805.

[5] C. Gonzalez and H. C. Van Ness, *J. Chem. Eng. Data*, 1983, **28**, 410-412.

[6] K. Nakanishi, N. Kato and M. Maruyama, *J. Phys. Chem.*, 1967, **71(4)**, 814-818.

[7] H. Geyer, P. Ulbig and M. Görnert, *J. Chem. Thermodynamics*, 2000, **32**, 1585-1596.

[8] M. Sakurai, *J. Chem. Eng. Data*, 1991, **36(4)**, 424–427.

[9] S. Dixit, J. Crain, W. C. K. Poon, J. L. Finney and A. K. Soper, *Nature*, 2002, **416**, 829-832.

[10] For negative ΔS^E, a decrease of volume during the mixing is another contributing factor. The contribution of the volume change is, however, minor (> ca. -30 J mol^{-1}) to the total ΔS^E (> ca. -700 J mol^{-1}), since the volume of an EG aqueous solution decreases by several % at most in the mixed process.

[11] Y. Ishihara, S. Okouchi and H Uedaira, *J. Chem. Soc., Faraday Trans.*, 1997, **93(18)**, 3337-3342.

[12] K. G. R. Pachler and P. L. Wessels, *J. Mol.Structure*, 1970, **6**, 471-478.

[13] K. Krishnan and R. S. Krishnan, *Proc. Ind. Acad. Sci. A*, 1966, **64**, 111-122.

[14] M. Matsugami, T. Takamuku, T. Otomo and T. Yamaguchi, *J. Phys. Chem. B*, 2006, **110**, 12372-12379.

[15] T. Hasegawa, In *Introduction to Experimental Infrared Spectroscopy*, ed. M. Tasumi, John Wiley & Sons: Chichester, 2014, pp 107-108.

[16] T. Sakabe, S. Yamazaki and T. Hasegawa, *J. Phys. Chem. B*, 2010, **114**, 6878-6885.

[17] J. Zhang, P. Zhang, F. H., Guohua Chen, L. Zhang, and X. Wei, *Ind. Eng. Chem. Res.*, 2009, **48**, 1287–1291.

[18] Although the CH_2 bending ($\delta(CH_2)$) vibration band of EG in ca. 1500-1100 cm^{-1} does not exhibit a significant shift, the chemometric analysis was performed in a range involving the $\delta(CH_2)$ region, since the skirt of the $\delta(OH_2)$ band in the lower side overwraps in the region.

[19] J. Diewok, A. de Juan, M. Maeder, R. Tauler and B. Lendl, *Anal. Chem.*, 2003, **75**, 641–647.

[20] P. J. Gemperline and E. Cash, *Anal. Chem.*, 2003, **75**, 4236–4243.

[21] W. Kessler and R. W. Kessler, *Anal. Bioanal. Chem.*, 2006, **384**, 1087–1095.

[22] R. Kjellander and E. Florin, *J. Chem. Soc., Faraday Trans. 1*, 1981, **77**, 2053-2077.

[23] The ALS calculation was performed with a little loosened constraint for the fast convergence, that is, the elements of the matrices of **K** and **C** are prohibited to have a smaller value than -0.001 and -0.01, respectively.

[24] T. Shimoaka and Y. Katsumoto, *J. Phys. Chem. A*, 2010, **114**, 11971–11976.